$Zn(OH)_2$-Functionalized Cellulose Acetate Butyrate Hybrid Microcapsules Incorporating Chromolaena odorata Extract: Structural Characterization, Thermal Behavior, and Antibacterial Properties

Jiraporn Ketwaraporn
Uttaradit Rajabhat University
Pongthep Jansanthea
pongthep.jan@uru.ac.th

Uttaradit Rajabhat University
Monthakan Boontheung
Uttaradit Rajabhat University
Suriyun Yimpin
Uttaradit Rajabhat University
Putthadee Ubolsook
Uttaradit Rajabhat University
Parinya Kraivuttinun
Uttaradit Rajabhat University

Research Article

Keywords: cellulose acetate butyrate, Chromolaena odorata extract, hybrid microcapsules, inorganic–organic hybrid materials, zinc hydroxide, antibacterial activity

Posted Date: June 12th, 2026

DOI: https://doi.org/10.21203/rs.3.rs-9935979/v1

Additional Declarations: No competing interests reported.

Abstract

$Zn(OH)_2$-functionalized cellulose acetate butyrate (CAB) hybrid microcapsules incorporating *Chromolaena odorata* extract were prepared and characterized as inorganic–organic hybrid materials. The microcapsules were fabricated by solvent evaporation followed by in situ precipitation of $Zn(OH)_2$ on the microcapsule surface. Structural, morphological, and thermal characteristics were investigated using X-ray diffraction (XRD), Fourier-transform infrared spectroscopy (FTIR), scanning electron microscopy coupled with energy-dispersive X-ray spectroscopy (SEM–EDS), particle size analysis, and thermogravimetric analysis (TGA). Antibacterial activity was evaluated against *Escherichia coli* and *Staphylococcus aureus* using minimum inhibitory concentration (MIC) and minimum bactericidal concentration (MBC) assays. The results demonstrated successful incorporation of $Zn(OH)_2$ into the CAB microcapsule system. XRD patterns revealed the presence of zinc-containing phases, while FTIR spectra indicated changes in the chemical environment of oxygen-containing functional groups following $Zn(OH)_2$ incorporation. SEM analysis showed increased surface roughness and particulate coverage with increasing $Zn(OH)_2$ content, and EDS confirmed the presence of zinc on the microcapsule surface. Particle size and thermal analyses further demonstrated that $Zn(OH)_2$ incorporation influenced the physicochemical characteristics of the hybrid microcapsules. Among the tested formulations, CAB–Zn–40 exhibited the strongest antibacterial activity, with MIC values of 12.8 mg mL^{-1} against *E. coli* and 6.4 mg mL^{-1} against *S. aureus*. The enhanced antibacterial performance was associated with the presence of Zn-containing surface domains and encapsulated bioactive constituents. These findings demonstrate that $Zn(OH)_2$ incorporation provides an effective strategy for producing CAB-based inorganic–organic hybrid microcapsules with tunable structural, thermal, and antibacterial properties.

1. Introduction

Cellulose-derived polymers have attracted considerable attention as sustainable materials for the development of functional hybrid systems because of their renewable origin, processability, and adaptable physicochemical characteristics [1]. Among these materials, cellulose acetate butyrate (CAB) is widely recognized as a versatile cellulose ester possessing favorable film-forming ability, tunable permeability, chemical stability, and compatibility with a broad range of organic and inorganic components [2]. Owing to these properties, CAB has been employed in encapsulation technologies, controlled-release systems, protective coatings, and hybrid material formulations designed for biomedical, environmental, and antimicrobial applications [3]. The ability of CAB to accommodate functional additives while maintaining structural integrity makes it a suitable matrix for the fabrication of multifunctional hybrid microcapsules.

In recent years, increasing attention has been directed toward the development of hybrid materials that combine polymeric matrices with biologically active compounds and inorganic constituents. Such hybrid systems offer opportunities to integrate multiple functionalities within a single material platform, including improved stability, enhanced physicochemical performance, and tailored biological activity [4]. The incorporation of natural products into polymer matrices is particularly attractive because plant-

derived compounds contain diverse secondary metabolites capable of providing antioxidant, antimicrobial, and therapeutic functions [5]. Encapsulation within polymer-based carriers may further improve the handling, storage stability, and utilization efficiency of these bioactive substances by reducing their exposure to external environmental conditions [6, 7].

Among the numerous medicinal plants investigated for material applications, *Chromolaena odorata* has emerged as a promising source of bioactive compounds. Extracts obtained from its leaves contain a variety of phytochemical constituents, including flavonoids, phenolic compounds, tannins, terpenoids, and other oxygenated organic molecules that have been associated with antibacterial, anti-inflammatory, antioxidant, and wound-healing activities [8]. These biological properties have stimulated growing interest in the incorporation of *C. odorata* extracts into functional materials, coatings, delivery systems, and antimicrobial formulations [9]. However, direct utilization of crude plant extracts may be limited by factors such as chemical instability, sensitivity to environmental conditions, volatilization of active components, and gradual degradation during storage. Consequently, encapsulation strategies have been increasingly explored to improve the preservation and utilization of plant-derived bioactive compounds within engineered material systems [10].

Parallel to the growing interest in natural bioactive compounds, inorganic zinc-containing materials have received considerable attention because of their distinctive physicochemical characteristics and reported antimicrobial properties [11]. Zinc-based compounds have been incorporated into a wide range of polymeric and hybrid materials to provide additional functionality while maintaining compatibility with organic matrices. Among these materials, zinc oxide has been extensively investigated; however, other zinc-containing phases have also attracted interest because variations in chemical composition, hydroxyl content, and surface characteristics may influence the structural organization and functional behavior of hybrid systems [12].

Zinc hydroxide, $Zn(OH)_2$, represents an inorganic material containing abundant hydroxyl groups that may contribute to the formation of hybrid architectures when introduced into organic matrices [13]. The presence of Zn-containing domains within polymer-based systems may influence particle morphology, structural organization, thermal behavior, and surface characteristics depending on the preparation method and inorganic loading level [14]. In addition, zinc-containing materials have frequently been associated with antibacterial performance, making them attractive candidates for incorporation into multifunctional hybrid materials designed for biological and environmental applications [15]. The integration of $Zn(OH)_2$ into polymeric microcapsules therefore offers an opportunity to combine the encapsulation capability of organic matrices with the physicochemical contributions of inorganic components.

The development of inorganic–organic hybrid microcapsules has emerged as an important research direction because such systems can integrate the advantages of both material classes within a single structure [16]. In these materials, the organic component commonly serves as a flexible and processable matrix capable of accommodating functional substances, whereas the inorganic component may

contribute to structural stability, surface modification, thermal resistance, or functional activity. The resulting hybrid microstructures often exhibit physicochemical characteristics that differ from those of their individual constituents, thereby expanding the range of potential applications [17]. For CAB-based systems, incorporation of inorganic phases may provide an effective route for tailoring morphology, thermal behavior, and biological performance while preserving the desirable processing characteristics of the cellulose-derived matrix.

Despite increasing interest in bio-based hybrid materials, limited information is available regarding $Zn(OH)_2$-functionalized CAB microcapsules containing plant-derived bioactive compounds. Previous studies have generally focused on either antibacterial activities of plant extracts or functional properties of zinc-containing materials independently, whereas investigations integrating both components within CAB-based hybrid microcapsules remain relatively scarce [18]. Furthermore, the influence of $Zn(OH)_2$ incorporation on the structural characteristics, morphology evolution, thermal behavior, and antibacterial performance of CAB microcapsules containing *C. odorata* extract has not been comprehensively examined. A better understanding of these aspects is important for the rational design of multifunctional inorganic–organic hybrid materials based on renewable polymer matrices.

Therefore, the present study investigated the preparation of CAB hybrid microcapsules incorporating *C. odorata* extract and subsequently functionalized with $Zn(OH)_2$ through an in situ precipitation approach. The resulting materials were evaluated using X-ray diffraction (XRD), Fourier-transform infrared spectroscopy (FTIR), scanning electron microscopy coupled with energy-dispersive spectroscopy (SEM–EDS), particle size analysis, thermogravimetric analysis (TGA), and antibacterial assays. Particular emphasis was placed on examining how $Zn(OH)_2$ incorporation influences the structural characteristics, chemical structure, morphology evolution, thermal behavior, and antibacterial performance of the resulting hybrid microcapsules. The study provides insight into the development of CAB-based inorganic–organic hybrid materials containing both plant-derived bioactive compounds and Zn-containing domains, thereby contributing to the broader understanding of multifunctional hybrid systems derived from renewable polymer resources.

2. Materials and Methods

2.1 Materials

All chemicals were analytical grade and used without further purification. Barium chloride dihydrate ($BaCl_2 \cdot 2H_2O$, ≥ 99.0%) was obtained from Elago Enterprises (Australia). Chloroform ($CHCl_3$, 99.8%) and ethanol (95%) were purchased from RCI LABSCAN (Thailand), while absolute ethanol (99.9%) was obtained from Duksan (Korea). Cellulose acetate butyrate (CAB, Mn ≈ 30,000) and dimethyl sulfoxide (DMSO, 99.9%) were supplied by VWR (UK). Poly(vinyl alcohol) (PVA, analytical reagent grade) was obtained from Chem-Supply (Australia), and zinc nitrate hexahydrate ($Zn(NO_3)_2 \cdot 6H_2O$, 98%) was obtained from Loba Chemie Pvt. Ltd. (India). Sulfuric acid (H_2SO_4, 98%), sodium chloride (NaCl, 99%), and sodium hydroxide (NaOH, 99%) were purchased from RCI LABSCAN. Nutrient broth and agar were obtained from

Himedia (India). All aqueous solutions were prepared using deionized (DI) water with conductivity < 1 µS/cm. Fresh *Chromolaena odorata* leaves were collected from the vicinity of Uttaradit Rajabhat University, Uttaradit Province, Thailand. Leaves were washed with DI water, air-dried under sunlight for 24–36 h, and finely chopped before extraction [18].

2.2 Preparation of C. odorata Leaf Extract

Air-dried *C. odorata* leaves were extracted using 95% ethanol at a solid-to-solvent ratio of 1:10 (w/v) under ambient conditions (25 ± 2°C) for 24 h with intermittent shaking. The mixture was homogenized and filtered sequentially through muslin cloth and Whatman No. 1 filter paper. The filtrate was concentrated under reduced pressure at 45°C and subsequently freeze-dried at − 55°C (0.04 mbar) to obtain dried extract powder. The resulting extract was stored in a desiccator until further use in microcapsule preparation.

2.3 Preparation of CAB Microcapsules

Cellulose acetate butyrate (CAB) was dissolved in 10 mL of ethyl acetate under magnetic stirring until a homogeneous solution was obtained. *C. odorata* extract prepared in Section 2.2 was added and stirred for 30 min to ensure uniform dispersion within the polymer phase. The organic phase was emulsified into 50 mL of 1% (w/v) poly(vinyl alcohol) (PVA) solution under stirring at 600 rpm to form an oil-in-water emulsion. Microcapsules were generated through solvent evaporation during CAB precipitation around the dispersed extract phase. The resulting suspension was centrifuged at 4,000 rpm for 10 min, washed three times with DI water, and air-dried at room temperature for 24 h.

2.4 $Zn(OH)_2$ Surface Modification of CAB Microcapsules

Dried CAB microcapsules (0.5 g) were dispersed in 50 mL of DI water under stirring at room temperature. Aqueous $Zn(NO_3)_2$ solutions at concentrations of 20–80 mmol/L were introduced to control Zn precursor concentration. Sodium hydroxide solution (0.1 M) was added dropwise until the suspension reached approximately pH 9.5 to induce in situ precipitation of $Zn(OH)_2$ on the microcapsule surface. The reaction was maintained for 60 min. The resulting products were collected by centrifugation at 4,000 rpm for 10 min, washed three times with DI water, and dried at 40°C for 24 h. Samples were designated CAB–Zn–10, CAB–Zn–20, CAB–Zn–30, and CAB–Zn–40 according to Zn precursor concentration.

2.5 Characterization Methods

X-ray diffraction (XRD; PANalytical X'Pert PRO, Cu Kα radiation, λ = 1.5406 Å) was employed to examine crystalline characteristics over a 2θ range of 10–80°. Fourier-transform infrared spectroscopy (FTIR; Bruker Tensor 27) was used to examine functional groups and chemical interactions within the samples over the range of 4000–400 cm^{-1}. Surface morphology and elemental distribution were evaluated using scanning electron microscopy coupled with energy-dispersive spectroscopy (SEM–EDS; Hitachi SU5000). Particle size and ζ-potential measurements were performed using a Malvern Zetasizer Nano

ZS. Thermogravimetric analysis (TGA; Mettler-Toledo TGA/DSC 1) was conducted under nitrogen atmosphere from 30–800°C at a heating rate of 10°C min^{-1}.

2.6 Antibacterial Evaluation

Antibacterial activity was evaluated against *Escherichia coli* (ATCC 25922) and *Staphylococcus aureus* (ATCC 25923). A broth microdilution method based on CLSI guidelines with slight modification for particulate samples was employed. Bacterial suspensions (approximately 1 × 10^6 CFU/mL) were exposed to serial dilutions of CAB–Zn–x microcapsules (x = 20–80 mmol/L Zn precursor) at final concentrations ranging from 0.8–25.6 mg/mL in 96-well plates. Following incubation at 37°C for 24 h, minimum inhibitory concentration (MIC) values were determined as the lowest concentration that prevented visible bacterial growth. Minimum bactericidal concentration (MBC) values were determined by plating aliquots from growth-inhibited wells onto nutrient agar. All experiments were performed in triplicate, and results were reported as mean MIC and MBC ± SD.

3. Results and Discussion

3.1 Structural Characteristics of $Zn(OH)_2$-Functionalized Hybrid Microcapsules

X-ray diffraction (XRD) analysis was performed to investigate the structural characteristics of $Zn(OH)_2$-functionalized CAB hybrid microcapsules and to evaluate the influence of $Zn(OH)_2$ incorporation on phase composition and crystallinity. The diffraction patterns presented in Fig. 1 reveal systematic changes in structural organization with increasing Zn precursor concentration. Distinct diffraction peaks observed for CAB–Zn–10 to CAB–Zn–40 at 2θ values of approximately 20.09°, 20.81°, 24.98°, 27.11°, 27.65°, and 32.73° are consistent with the characteristic reflections of orthorhombic $Zn(OH)_2$ (JCPDS No. 01-076-1778) [19]. The appearance of these reflections confirms the successful formation of Zn-containing crystalline domains within the hybrid microcapsule system.

The diffraction pattern of the unmodified microcapsules (CAB–Zn–0) was dominated by a broad halo, indicating the predominantly amorphous nature of the CAB matrix and encapsulated phytochemical constituents. Following $Zn(OH)_2$ incorporation, additional diffraction features became progressively more pronounced. At the lowest Zn precursor concentration (CAB–Zn–10), the $Zn(OH)_2$-related reflections were relatively broad and exhibited low intensity, suggesting the presence of limited amounts of crystalline Zn-containing phases. As the Zn precursor concentration increased from CAB–Zn–20 to CAB–Zn–40, the diffraction peaks became sharper and more intense, indicating an increase in the relative crystalline contribution of $Zn(OH)_2$ within the hybrid microcapsules [20].

The gradual enhancement of diffraction intensity with increasing Zn content suggests progressive incorporation and deposition of $Zn(OH)_2$ throughout the microcapsule system. Similar behavior has been reported in inorganic–organic hybrid materials, where increasing inorganic content contributes to the development of more distinguishable crystalline features within an otherwise amorphous matrix [21].

The coexistence of broad amorphous backgrounds and well-defined $Zn(OH)_2$ reflections indicates that the resulting materials retained the characteristic amorphous nature of the CAB-based matrix while simultaneously incorporating crystalline Zn-containing domains.

The observed structural evolution is therefore consistent with the formation of $Zn(OH)_2$-functionalized hybrid microcapsules containing both organic and inorganic structural components. Increasing $Zn(OH)_2$ concentration resulted in a greater crystalline contribution from the inorganic phase, leading to measurable changes in the overall diffraction profile. These findings demonstrate that $Zn(OH)_2$ incorporation influenced the structural organization of the hybrid microcapsules and contributed to the development of an inorganic–organic hybrid material with composition-dependent crystalline characteristics.

3.2 Chemical Structure and Functional Group Analysis

FTIR spectroscopy was employed to evaluate the chemical structure and functional groups present in the *C. odorata* extract, CAB microcapsules, and $Zn(OH)_2$-functionalized hybrid microcapsules. The corresponding spectra are presented in Fig. 2. The crude extract exhibited a broad absorption band centered at approximately 3317 cm^{-1}, which is attributed to O–H stretching vibrations of hydroxyl-containing phytochemicals. Additional absorption bands observed at 1618, 1512, and 1348 cm^{-1} are associated with aromatic C = C vibrations and C–N/C–O stretching modes characteristic of phenolic and flavonoid-related constituents commonly reported in *C. odorata* extracts [22, 23].

The spectrum of the unmodified microcapsules (CAB–Zn–0) retained the principal absorption features of both the CAB matrix and the encapsulated extract. Broad O–H stretching bands in the region of 3400 cm^{-1} and ester carbonyl absorptions within the 1700–1600 cm^{-1} region remained clearly detectable, indicating that the encapsulation process preserved the major functional groups of the incorporated bioactive compounds within the polymer matrix [24]. No additional absorption bands were observed following microcapsule formation, suggesting that encapsulation predominantly involved physical entrapment of the extract within the CAB matrix together with non-covalent interactions among the constituent components.

Following $Zn(OH)_2$ incorporation (CAB–Zn–40), noticeable changes in spectral intensity were observed, particularly in the O–H stretching and carbonyl-associated regions. In addition, absorption bands appearing at approximately 715 and 545 cm^{-1} can be assigned to Zn–O vibrational modes, indicating the presence of zinc-containing species within the hybrid microcapsules [25]. The reduction in intensity of oxygen-containing functional group bands together with the emergence of Zn–O-related absorptions suggests possible interactions between Zn-containing domains and hydroxyl- or carbonyl-bearing components present in both the CAB matrix and the encapsulated phytochemicals. These spectral changes are consistent with the incorporation of an inorganic phase into the organic microcapsule structure and support the formation of an inorganic–organic hybrid material.

The overall FTIR results indicate that $Zn(OH)_2$ incorporation modified the chemical environment of selected functional groups within the hybrid microcapsules while preserving the fundamental chemical structure of the CAB matrix and encapsulated extract. The observed spectral variations may be associated with changes in the distribution and local environment of oxygen-containing functional groups after $Zn(OH)_2$ deposition. Such modifications are consistent with the formation of Zn-containing domains within the hybrid microcapsule architecture and may contribute to subsequent changes in morphological characteristics, thermal behavior, and antibacterial performance discussed in later sections.

3.3 Morphological Evolution and Elemental Composition

3.3.1 EDS Analysis

Energy-dispersive X-ray spectroscopy (EDS) was employed to evaluate the elemental composition of the $Zn(OH)_2$-functionalized CAB hybrid microcapsules and to verify the presence of zinc-containing domains within the hybrid material (Fig. 3). The spectra of all formulations were dominated by carbon (C) and oxygen (O) signals, which are characteristic of the cellulose acetate butyrate matrix and the encapsulated plant-derived constituents. Following $Zn(OH)_2$ incorporation, distinct Zn signals were observed in the modified samples, confirming the presence of zinc-containing components within the microcapsule system. These observations are consistent with the established use of EDS for elemental identification and compositional assessment of hybrid materials [26].

In addition to the major elements, minor signals corresponding to gold (Au) and sodium (Na) were detected. The Au signal originated from the sputter-coating process used during SEM sample preparation, whereas the Na signal may be associated with residual precursor species or traces remaining after the washing procedure. Owing to their low abundance and experimental origin, these elements were not considered integral components of the hybrid microcapsule structure.

Quantitative EDS analysis revealed a gradual increase in Zn content with increasing precursor concentration. CAB–Zn–10 and CAB–Zn–20 exhibited relatively low Zn levels (approximately 0.1 wt%), whereas CAB–Zn–30 and CAB–Zn–40 showed substantially higher Zn contents approaching 0.5 wt%. The concentration-dependent increase in Zn abundance indicates progressive incorporation of zinc-containing domains during the precipitation process.

The compositional trend observed by EDS is consistent with the structural and morphological changes identified by XRD and SEM analyses. As the concentration of the zinc precursor increased, a corresponding increase in surface-associated Zn-containing domains was observed, suggesting more extensive incorporation of the inorganic component within the hybrid microcapsule architecture [27]. The increasing Zn content may contribute to variations in the physicochemical characteristics of the hybrid material, including thermal behavior and antibacterial performance.

Overall, EDS analysis confirms successful Zn incorporation into the CAB-based microcapsules and supports the formation of an inorganic–organic hybrid material. Furthermore, the results demonstrate that the Zn content can be adjusted through precursor concentration, providing a controllable approach for tailoring the composition and functional characteristics of the hybrid microcapsule system.

3.3.2 SEM Analysis

Scanning electron microscopy (SEM) was used to investigate the morphological evolution of CAB microcapsules following $Zn(OH)_2$ functionalization (Fig. 4). The unmodified sample (CAB–Zn–0) exhibited predominantly spherical particles with relatively smooth surfaces, indicating successful microcapsule formation and a comparatively uniform external morphology. No distinct particulate deposits were observed on the particle surface, suggesting that the morphology was primarily governed by the polymeric matrix.

Following $Zn(OH)_2$ incorporation, noticeable changes in surface morphology were observed. CAB–Zn–10 displayed localized surface irregularities together with the appearance of discrete particulate features distributed across the microcapsule surface. These features suggest the initial formation of Zn-containing domains associated with the external region of the hybrid microcapsules. Increasing the precursor concentration to 20 mM resulted in more extensive particulate coverage and a reduction in surface uniformity, indicating progressive incorporation of the inorganic component within the hybrid system [28].

More pronounced morphological changes were observed at higher $Zn(OH)_2$ concentrations. CAB–Zn–30 exhibited densely distributed particulate structures across the microcapsule surface, while CAB–Zn–40 showed extensive surface coverage accompanied by increased roughness and the presence of aggregated surface features. The gradual increase in particulate density and surface roughness across the series is consistent with concentration-dependent accumulation of Zn-containing domains on the microcapsule exterior [29].

The observed morphological evolution corresponds well with the compositional results obtained from EDS analysis and the structural changes identified by XRD. Together, these findings indicate that increasing precursor concentration promotes greater incorporation of the inorganic phase and modifies the external morphology of the hybrid microcapsules. The development of rougher and more heterogeneous surfaces may increase the exposure of Zn-containing regions and contribute to changes in the overall physicochemical characteristics of the material [30].

Overall, SEM observations demonstrate that $Zn(OH)_2$ incorporation significantly influences the morphology of the CAB microcapsules. The progressive transformation from smooth polymeric particles to rough, particulate-covered structures supports the formation of inorganic–organic hybrid microcapsules with composition-dependent structural organization.

3.4 Particle Size Characteristics of $Zn(OH)_2$-Functionalized Hybrid Microcapsules

Particle-size distribution profiles of *C. odorata*-loaded CAB microcapsules functionalized with different $Zn(OH)_2$ concentrations are presented in Fig. 5, and the corresponding mean particle diameters are summarized in Table 1. The average particle size increased progressively with increasing Zn precursor concentration, indicating that $Zn(OH)_2$ incorporation influenced the dimensional characteristics of the hybrid microcapsules. Unmodified microcapsules (CAB–Zn–0) exhibited a mean particle diameter of 1013.3 ± 66.5 nm, whereas the highest $Zn(OH)_2$ loading (CAB–Zn–40) produced microcapsules with an average diameter of 1275.3 ± 109.9 nm.

The gradual increase in particle size may be associated with the formation and accumulation of Zn-containing domains on the microcapsule surface during the precipitation process. Similar increases in particle dimensions have been reported for inorganic-modified polymeric systems, where deposition of inorganic species contributes to enlargement of the overall particle structure [31]. Relatively small changes were observed at lower Zn precursor concentrations, whereas more pronounced increases occurred at higher precursor levels, suggesting that the extent of $Zn(OH)_2$ incorporation increased with precursor availability.

The particle-size distribution profiles further demonstrate that $Zn(OH)_2$ functionalization affected the physical characteristics of the microcapsules. The progressive increase in average particle diameter is consistent with the development of an inorganic–organic hybrid microstructure in which Zn-containing domains become increasingly associated with the CAB-based microcapsules. This behavior may reflect increased surface coverage by precipitated $Zn(OH)_2$ and localized accumulation of inorganic material as the precursor concentration increased. Similar trends have been observed in precipitation-mediated hybrid material systems, where higher precursor loading promotes greater incorporation of inorganic components into polymer-based matrices [32].

The observed dimensional changes are also consistent with the morphological features identified by SEM analysis, which revealed increasing surface roughness and the presence of inorganic deposits with increasing $Zn(OH)_2$ concentration. Collectively, the particle-size and morphological data suggest successful incorporation of $Zn(OH)_2$ into the CAB microcapsule system, resulting in the formation of hybrid microcapsules with modified physicochemical characteristics.

Table 1
Particle size and thermal degradation characteristics of $Zn(OH)_2$-functionalized CAB hybrid microcapsules prepared with different Zn precursor concentrations. Variations in particle dimensions and thermal degradation parameters indicate that $Zn(OH)_2$ incorporation influenced the physicochemical characteristics of the hybrid microcapsule system.

Sample	Mean Particle Size (nm)	Initial Onset Temperature (°C)	Final Onset Temperature (°C)	Weight Loss (%)
CAB–Zn–0	1013.3 ± 66.5	336.7	385.3	85.90
CAB–Zn–10	1049.5 ± 74.5	252.6	368.8	48.94
CAB–Zn–20	1159.8 ± 58.8	292.8	371.2	37.57
CAB–Zn–30	1202.5 ± 82.8	274.4	371.3	28.33
CAB–Zn–40	1275.3 ± 109.9	287.0	367.8	28.05

3.5 Thermal Behavior of Hybrid Microcapsules

Thermogravimetric analysis was performed to evaluate the influence of $Zn(OH)_2$ incorporation on the thermal behavior of CAB-based hybrid microcapsules. The corresponding thermograms and degradation parameters are presented in Fig. 6 and Table 1. All formulations exhibited a major degradation region within the temperature range of approximately 250–400°C, which is primarily associated with decomposition of the CAB matrix together with degradation of encapsulated phytochemical constituents.

The uncoated formulation (CAB–Zn–0) exhibited the highest overall mass loss (85.90%) and an onset degradation temperature of 336.7°C. Following incorporation of $Zn(OH)_2$, progressive reductions in total mass loss were observed. CAB–Zn–10 showed a lower onset degradation temperature (252.6°C), while the corresponding decrease in weight loss to 48.94% suggests that the presence of Zn-containing domains influenced the thermal decomposition behavior of the hybrid microcapsules. Further increases in $Zn(OH)_2$ content resulted in additional reductions in mass loss, reaching 37.57%, 28.33%, and 28.05% for CAB–Zn–20, CAB–Zn–30, and CAB–Zn–40, respectively. In addition, CAB–Zn–40 exhibited an onset degradation temperature of 287.0°C, indicating changes in thermal response with increasing $Zn(OH)_2$ incorporation.

The concentration-dependent decrease in mass loss demonstrates that incorporation of $Zn(OH)_2$ modified the thermal degradation characteristics of the hybrid microcapsules [33]. The presence of inorganic Zn-containing domains may contribute to changes in decomposition behavior by altering heat transfer processes and influencing the distribution of thermally labile components within the hybrid structure [34]. The progressively lower mass losses observed with increasing $Zn(OH)_2$ content are

consistent with the increasing proportion of thermally stable inorganic material remaining after thermal treatment. Similar behavior has been reported in zinc-containing hybrid systems, where inorganic phases contributed to enhanced residual mass and modified degradation profiles during thermal analysis.

The thermal behavior observed in this study is also consistent with the structural and morphological characteristics identified by XRD and SEM analyses. The formation of Zn-containing domains on the microcapsule surface, together with changes in crystalline features, suggests the development of an inorganic–organic hybrid microstructure that may influence thermal decomposition pathways. Although the precise mechanisms cannot be established from the present data, the combined characterization results indicate that $Zn(OH)_2$ incorporation contributed to measurable changes in the thermal stability and degradation characteristics of the CAB-based hybrid microcapsules.

Overall, the TGA results demonstrate that increasing $Zn(OH)_2$ content altered the thermal behavior of the microcapsules and reduced the extent of mass loss during thermal degradation. These findings support the role of $Zn(OH)_2$ as an important inorganic component within the hybrid system and highlight its contribution to the physicochemical characteristics of the resulting inorganic–organic hybrid microcapsules.

3.6 Antibacterial Activity of $Zn(OH)_2$-Functionalized Hybrid Microcapsules

The antibacterial activity of $Zn(OH)_2$-functionalized CAB hybrid microcapsules incorporating *Chromolaena odorata* extract was evaluated against *Escherichia coli* and *Staphylococcus aureus* using minimum inhibitory concentration (MIC) and minimum bactericidal concentration (MBC) assays. The results demonstrated that antibacterial performance varied according to $Zn(OH)_2$ loading, indicating that incorporation of Zn-containing domains influenced the biological response of the hybrid microcapsules. As summarized in Table 2, antibacterial activity was dependent on microcapsule composition and did not increase strictly in proportion to $Zn(OH)_2$ content, suggesting that both inorganic incorporation and microcapsule characteristics contributed to the observed antibacterial behavior.

3.6.1 Minimum Inhibitory Concentration (MIC)

The MIC values of the hybrid microcapsules are presented in Fig. 7. A gradual decrease in MIC was observed with increasing $Zn(OH)_2$ loading, with CAB–Zn–40 exhibiting the strongest inhibitory activity against both bacterial strains. The lowest MIC values were 12.8 mg/mL for *E. coli* and 6.4 mg/mL for *S. aureus*. In contrast, formulations containing lower amounts of $Zn(OH)_2$ generally required higher concentrations to suppress bacterial growth.

Differences in bacterial susceptibility were evident throughout the study. For most formulations, *S. aureus* exhibited lower MIC values than *E. coli*, indicating greater sensitivity to the hybrid microcapsules. This observation may be associated with differences in cell envelope architecture between Gram-

positive and Gram-negative bacteria. The additional outer membrane present in Gram-negative bacteria may reduce accessibility of external antimicrobial agents and thereby contribute to lower susceptibility [35].

The progressive reduction in MIC values with increasing $Zn(OH)_2$ loading suggests that incorporation of Zn-containing domains influenced the antibacterial characteristics of the hybrid microcapsules. The improved inhibitory performance observed in CAB–Zn–30 and CAB–Zn–40 may be associated with increased availability of surface Zn species and modifications in microcapsule surface characteristics [36]. However, MIC measurements alone do not provide direct evidence regarding the underlying antibacterial mechanism, and therefore only indicate concentration-dependent inhibitory activity.

3.6.2 Minimum Bactericidal Concentration (MBC)

The MBC values of the hybrid microcapsules are summarized in Table 2, while representative bacterial growth patterns are shown in Fig. 8. Overall, the bactericidal response followed a trend similar to that observed for MIC. CAB–Zn–40 exhibited the strongest bactericidal performance, with MBC values of 12.8 mg/mL against *E. coli* and 6.4 mg/mL against *S. aureus*. Formulations containing lower $Zn(OH)_2$ loadings generally required higher concentrations to achieve complete bacterial inactivation.

Interestingly, CAB–Zn–10 and CAB–Zn–20 exhibited higher MBC values against *E. coli* than CAB–Zn–0, indicating that partial incorporation of $Zn(OH)_2$ did not necessarily result in enhanced bactericidal performance. This behavior suggests that antibacterial efficacy was influenced by multiple factors related to hybrid microcapsule composition rather than solely by the amount of inorganic material present. Variations in the distribution and accessibility of Zn-containing domains within the hybrid structure may have contributed to these differences [37].

Among all formulations, CAB–Zn–30 and CAB–Zn–40 demonstrated substantially improved bactericidal activity, particularly against *S. aureus*, where MBC values decreased to 12.8 and 6.4 mg/mL, respectively. The consistently lower MBC values observed for *S. aureus* compared with *E. coli* were in agreement with the MIC results and further support the greater susceptibility of the Gram-positive bacterium toward the tested hybrid microcapsules.

The enhanced bactericidal performance observed at higher $Zn(OH)_2$ loadings may be associated with the combined presence of Zn-containing domains and bioactive phytochemical constituents originating from *C. odorata* extract [38]. Previous studies have reported antibacterial activity for zinc-based materials and phytochemical compounds derived from medicinal plants [15]. Nevertheless, the present study did not directly evaluate ion-release behavior, reactive oxygen species generation, membrane damage, or other antibacterial pathways. Therefore, any contribution of these factors should be considered a possible explanation rather than a confirmed mechanism.

Overall, the antibacterial results demonstrate that incorporation of $Zn(OH)_2$ influenced the antibacterial performance of CAB-based hybrid microcapsules. The concentration-dependent reduction in MIC and MBC values, particularly for CAB–Zn–30 and CAB–Zn–40, indicates that $Zn(OH)_2$ loading played an

important role in determining biological activity. The observed variations among formulations further suggest that optimization of inorganic content is necessary to achieve effective antibacterial performance in this inorganic–organic hybrid microcapsule system.

Table 2
Minimum bactericidal concentration (MBC) values of CAB microcapsules against *E. coli* and *S. aureus*. Differences in MBC values among formulations indicate variations in antibacterial activity associated with changes in microcapsule composition and $Zn(OH)_2$ content.

Microcapsule Type	MBC (*E. coli*) (mg/mL)	MBC (*S. aureus*) (mg/mL)
CAB-Zn-0	25.6	25.6
CAB-Zn-10	51.2	51.2
CAB-Zn-20	51.2	25.6
CAB-Zn-30	25.6	12.8
CAB-Zn-40	12.8	6.4

3.7 Proposed Hybrid Material Formation

Based on the combined XRD, FTIR, SEM, EDS, particle size, and antibacterial results, a conceptual model for the formation of the $Zn(OH)_2$-functionalized CAB hybrid microcapsules is proposed, as illustrated in Fig. 9. The model suggests that the hybrid microcapsules possess a core–shell architecture (Fig. 9a) consisting of a cellulose acetate butyrate (CAB) matrix that encapsulates *Chromolaena odorata* extract within the interior region (Fig. 9b,d), while $Zn(OH)_2$-rich domains are distributed over the external surface of the microcapsules (Fig. 9c). This structural arrangement is consistent with the fabrication process, in which CAB-based microcapsules were initially formed and subsequently modified through $Zn(OH)_2$ deposition [39].

The proposed hybrid structure is supported by the physicochemical characterization results. XRD analysis revealed the appearance and increased intensity of diffraction features associated with zinc-containing phases, indicating successful incorporation of $Zn(OH)_2$ into the microcapsule system [40]. In addition, FTIR spectra showed variations in characteristic absorption bands of CAB and extract-derived functional groups, suggesting changes in the local chemical environment after $Zn(OH)_2$ deposition [41]. As illustrated in Fig. 9e, these changes may be associated with physical interactions involving hydroxyl, carbonyl, and other oxygen-containing groups within the hybrid structure. However, the available evidence does not allow definitive identification of specific bonding mechanisms.

Morphological observations further support the proposed architecture. SEM images showed that $Zn(OH)_2$ incorporation increased surface roughness and particulate coverage, while EDS analysis confirmed the presence of zinc on the microcapsule surface [42]. These findings are consistent with the formation of surface-associated $Zn(OH)_2$ domains (Fig. 9c), resulting in a heterogeneous inorganic–

organic hybrid structure. The proposed model may also explain the observed changes in particle size, thermal behavior, and antibacterial performance. Increasing $Zn(OH)_2$ content could contribute to larger particle dimensions and modified thermal stability while providing additional Zn-containing surface regions that may participate in antibacterial activity [43]. Although the antibacterial mechanism was not directly investigated, the enhanced activity of the $Zn(OH)_2$-functionalized formulations may be associated with the combined effects of the surface-deposited $Zn(OH)_2$ domains and the bioactive phytochemical constituents retained within the encapsulated *C. odorata* extract.

Overall, the available experimental evidence supports the formation of an inorganic–organic hybrid microcapsule system in which CAB serves as the structural matrix, *C. odorata* extract functions as the bioactive component, and $Zn(OH)_2$ provides inorganic surface functionality, collectively contributing to the physicochemical and antibacterial characteristics of the hybrid microcapsules.

4. Conclusions

$Zn(OH)_2$-functionalized cellulose acetate butyrate (CAB) hybrid microcapsules incorporating *Chromolaena odorata* extract were successfully prepared and evaluated as inorganic–organic hybrid materials. The incorporation of $Zn(OH)_2$ produced concentration-dependent changes in the structural, morphological, thermal, and antibacterial characteristics of the microcapsule system. Combined XRD, FTIR, SEM–EDS, particle size, and TGA analyses demonstrated that the presence of Zn-containing domains influenced the structural organization, surface morphology, particle characteristics, and thermal behavior of the hybrid microcapsules. The observed changes are consistent with the formation of a heterogeneous inorganic–organic hybrid architecture in which $Zn(OH)_2$ was incorporated into the CAB-based microcapsule system.

Structural characterization revealed progressive modification of microcapsule morphology and surface features with increasing $Zn(OH)_2$ content, while FTIR and XRD analyses suggested the coexistence of organic and inorganic components within the hybrid material. Thermal analysis further indicated that $Zn(OH)_2$ incorporation altered the degradation behavior of the microcapsules, demonstrating that inorganic incorporation contributed to changes in the physicochemical characteristics of the system. These findings collectively show that $Zn(OH)_2$ incorporation can serve as an effective approach for tailoring the structural and thermal properties of CAB-based hybrid microcapsules.

Variations in structural and thermal characteristics were accompanied by changes in antibacterial performance. Among the investigated formulations, CAB–Zn–40 exhibited the strongest antibacterial activity against *Escherichia coli* and *Staphylococcus aureus*. The enhanced antibacterial response may be associated with concentration-dependent changes in surface morphology, the presence of Zn-containing domains, and possible interactions between inorganic and phytochemical components within the hybrid microcapsules. However, the precise antibacterial mechanisms were not directly investigated and therefore require further study.

Overall, the present work demonstrates that $Zn(OH)_2$ incorporation provides a practical strategy for producing CAB-based inorganic–organic hybrid microcapsules with tunable physicochemical and antibacterial properties. The findings contribute to the understanding of Zn-containing hybrid materials derived from bio-based polymer systems and support their potential for future functional material applications. Future investigations should focus on release behavior, long-term stability, biodegradation characteristics, biocompatibility, and application-specific performance to further define the capabilities and limitations of these hybrid materials.

Declarations

Acknowledgements

We sincerely appreciate the generous support provided by the Thailand Scientific Research and Innovation (TSRI) for this study.

Ethical Approval

Not applicable.

Consent for publication

Not applicable.

Competing interest

The authors declare no conflicts of interest, whether personal relationships or financial considerations, that could have influenced the publication of this study.

Funding

No funding was received to assist with the preparation of this manuscript.

Data availability

The data are available from the corresponding author upon reasonable request.

Author Contributions Statement

J.K. supervised the study and contributed to conceptualization, methodology, and writing (original draft, review, and editing). **P.J.** led conceptualization, methodology, writing (original draft, review, and editing). **M.B.** and **S.Y.** contributed to methodology, investigation, validation. **P.U.** performed investigation and validation. **P.K.** contributed to conceptualization, methodology, investigation, validation. All authors reviewed and approved the final manuscript.

References

1. M.V. Silva, Y.E. Serge-Correales, L.H. Pereira, H. da S. Barud, S.J. Ribeiro, H. Otaguro, R.M.D. Assunção, ACS Omega 10, 18125–18134 (2025). https://doi.org/10.1021/acsomega.5c02294
2. E.M. Khaing, N. Lertsuphotvanit, W. Thammasut, C. Rojviriya, S. Chansatidkosol, S. Phattarateera, W. Pichayakorn, T. Phaechamud, Polymers 16, 3477 (2024). https://doi.org/10.3390/polym16243477
3. D. Parajuli, Front. Chem. 12, 1400375 (2024). https://doi.org/10.3389/fchem.2024.1400375
4. R. Sreena, G. Raman, G. Manivasagam, A.J. Nathanael, J. Mater. Chem. B 12, 11278–11301 (2024). https://doi.org/10.1039/D4TB01525H
5. F. Olawale, K. Olofinsan, O. Iwaloye, S. Afr. J. Bot. 144, 44–57 (2022). https://doi.org/10.1016/j.sajb.2021.09.001
6. V. Pérez-Pérez, C. Jiménez-Martínez, J.L. González-Escobar, L.J. Corzo-Ríos, Front. Chem. 12, 1423500 (2024). https://doi.org/10.3389/fchem.2024.1423500
7. A. Rezagholizade-Shirvan, M. Soltani, S. Shokri, R. Radfar, M. Arab, E. Shamloo, Food Chem. X 24, 101953 (2024). https://doi.org/10.1016/j.fochx.2024.101953
8. M.A. Yanis, M. Amirsyah, A.D. Harsono, J. Penelit. Pendidik. IPA 10, 10670–10676 (2024). https://doi.org/10.29303/jppipa.v10i12.9423
9. M. Abdul Latif, A. Mustafa, L.C. Keong, A. Hamid, PLoS One 19, e0295381 (2024). https://doi.org/10.1371/journal.pone.0295381
10. F. Cui, H. Zhang, D. Wang, X. Tan, X. Li, Y. Li, J. Li, T. Li, Food Funct. 14, 6766–6783 (2023). https://doi.org/10.1039/D3FO01077E
11. C.R. Mendes, G. Dilarri, C.F. Forsan, V.D.M.R. Sapata, P.R.M. Lopes, P.B. de Moraes, R.N. Montagnolli, H. Ferreira, E.D. Bidoia, Sci. Rep. 12, 2658 (2022). https://doi.org/10.1038/s41598-022-06617-2
12. M. Arif, A. Rauf, T. Akhter, Int. J. Biol. Macromol. 274(Pt 1), 133250 (2024). https://doi.org/10.1016/j.ijbiomac.2024.133250
13. B. Somtürk Yilmaz, J. Inorg. Organomet. Polym. Mater. 34, 5329–5341 (2024). https://doi.org/10.1007/s10904-024-03169-2
14. M. Srivastava, K.R. Singh, T. Singh, M. Asiri, M. Suliman, H. Sabia, P.R. Deen, R. Chaube, R. Singh, Int. J. Biol. Macromol. 253, 126886 (2023). https://doi.org/10.1016/j.ijbiomac.2023.126886
15. J. Nan, Y. Chu, R. Guo, P. Chen, Front. Mater. 11, 1449614 (2024). https://doi.org/10.3389/fmats.2024.1449614
16. J. Song, A.S. Vikulina, B.V. Parakhonskiy, A.G. Skirtach, Front. Chem. 11, 1078840 (2023). https://doi.org/10.3389/fchem.2023.1078840
17. H. Lin, W. Liu, X. Wu, Crystals 14, 535 (2024). https://doi.org/10.3390/cryst14060535
18. J. Ketwaraporn, S. Pinthong, R. Kerdphu, S. Daebau, P. Kraivuttinun, P. Jansanthea, Indones. J. Chem. 24, 1527–1540 (2024). https://doi.org/10.22146/ijc.95841

19. A. Gordeeva, Y.J. Hsu, I.Z. Jenei, P.H.B. Carvalho, S.I. Simak, O. Andersson, U. Häussermann, ACS Omega 5, 17617–17627 (2020). https://doi.org/10.1021/acsomega.0c02075
20. S.T. Gobena, A.D. Woldeyonnes, Discover Mater. 4, 52 (2024). https://doi.org/10.1007/s43939-024-00119-0
21. S.X. Drakopoulos, J. Wu, S.M. Maguire, S. Srinivasan, K. Randazzo, E.C. Davidson, R.D. Priestley, Prog. Polym. Sci. 156, 101870 (2024). https://doi.org/10.1016/j.progpolymsci.2024.101870
22. S. Agatonovic-Kustrin, V. Gegechkori, D.S. Petrovich, K.T. Ilinichna, D.W. Morton, Molecules 26, 6892 (2021). https://doi.org/10.3390/molecules26226892
23. R.M. Aldahasi, A. Shami, A.E. Mohammed, PeerJ 12, e17023 (2024). https://doi.org/10.7717/peerj.17023
24. F. Seke, O.Q. Adiamo, Y. Sultanbawa, D. Sivakumar, Foods 12, 4045 (2023). https://doi.org/10.3390/foods12214045
25. M. Faheem, H.M. Siddiqi, A. Habib, M. Shahid, A. Afzal, Front. Environ. Sci. 10, 965925 (2022). https://doi.org/10.3389/fenvs.2022.965925
26. I.R. Tay, J. Xue, W.S.V. Lee, Adv. Sci. (Weinh.) 10, e2303211 (2023). https://doi.org/10.1002/advs.202303211
27. S. Muhammad, F. Batool, M. Irfan, M. Ahmad, BME Horiz. 1, 76 (2023). https://doi.org/10.37155/2972-449X-vol1(2)-76
28. J. Lin, M. Kilani, M. Baharfar, R. Wang, G. Mao, Nanoscale 16, 19564–19588 (2024). https://doi.org/10.1039/D4NR02389G
29. A.I. Oliva, I.J. González-Chan, P.E. Várguez, A.I. Trejo-Ramos, A.I. Oliva-Avilés, Surf. Eng. 38, 907–929 (2023). https://doi.org/10.1080/02670844.2023.21878
30. Y. Yang, H. Tian, S. Napolitano, B. Zuo, Prog. Polym. Sci. 144, 101725 (2023). https://doi.org/10.1016/j.progpolymsci.2023.101725
31. Y. Yu, K. Liu, J. Chen, L. Mi, A. Feng, Y. Yu, F. Xiao, ACS Appl. Nano Mater. 7, 20114–20122 (2024). https://doi.org/10.1021/acsanm.4c02871
32. A.D. Malla, J.H. Sullivan, D.J. Penney, M. Goldsworthy, D. Britton, G. Williams, F. Goodwin, A.P. Cardoso, npj Mater. Degrad. 8, 78 (2024). https://doi.org/10.1038/s41529-024-00494-2
33. A.D. Zena, S. Periyasamy, M. Tesfaye, Z. Tumssa, B.A. Mohamed, V. Karthik, P. Asaithambi, D. Getachew, T.M. Aminabhavi, J. Taiwan Inst. Chem. Eng. 166, 105488 (2025). https://doi.org/10.1016/j.jtice.2024.105488
34. C.V. Ruiz, M.E. Becerra, O. Giraldo, Nanomaterials 10, 163 (2020). https://doi.org/10.3390/nano10010163
35. S.B. Ghaffari, M.H. Sarrafzadeh, M. Salami, A. Alvandi, J. Drug Deliv. Sci. Technol. 91, 105221 (2024). https://doi.org/10.1016/j.jddst.2023.105221
36. A.T. Reda, J.Y. Park, Y.T. Park, J. Funct. Biomater. 15, 103 (2024) https://doi.org/10.3390/jfb15040103

37. J. Awassa, S. Soulé, D. Cornu, C. Ruby, S. El-Kirat-Chatel, Nanoscale 14, 10335–10348 (2022) https://doi.org/10.1039/D2NR02395D
38. M. Shandhiya, B. Janarthanan, S. Sharmila, Arch. Microbiol. 206, 52 (2024) https://doi.org/10.1007/s00203-023-03743-1
39. B. Jiang, M. Mu, Y. Zhou, J. Zhang, W. Li, Small 20, 2311897 (2024) https://doi.org/10.1002/smll.202311897
40. A.V. Rodrigues, B.S.D. Onishi, S.J.L. Ribeiro, ChemPhysChem 24, e202300134 (2023) https://doi.org/10.1002/cphc.202300134
41. L. Demelius, L. Zhang, A.M. Coclite, M.D. Losego, Mater. Adv. 5, 8464–8474 (2024) https://doi.org/10.1039/D4MA00733F
42. I. Rezić, Š. Skoc, M. Majdak, S. Jurić, K.S. Stracenski, M. Vinceković, Polymers 14, 1961 (2022) https://doi.org/10.3390/polym14101961
43. B. Farasati Far, M.R. Naimi-Jamal, M. Jahanbakhshi, A. Hadizadeh, S. Dehghan, S. Hadizadeh, Sci. Rep. 14, 7505 (2024) https://doi.org/10.1038/s41598-024-58174-9

Figures

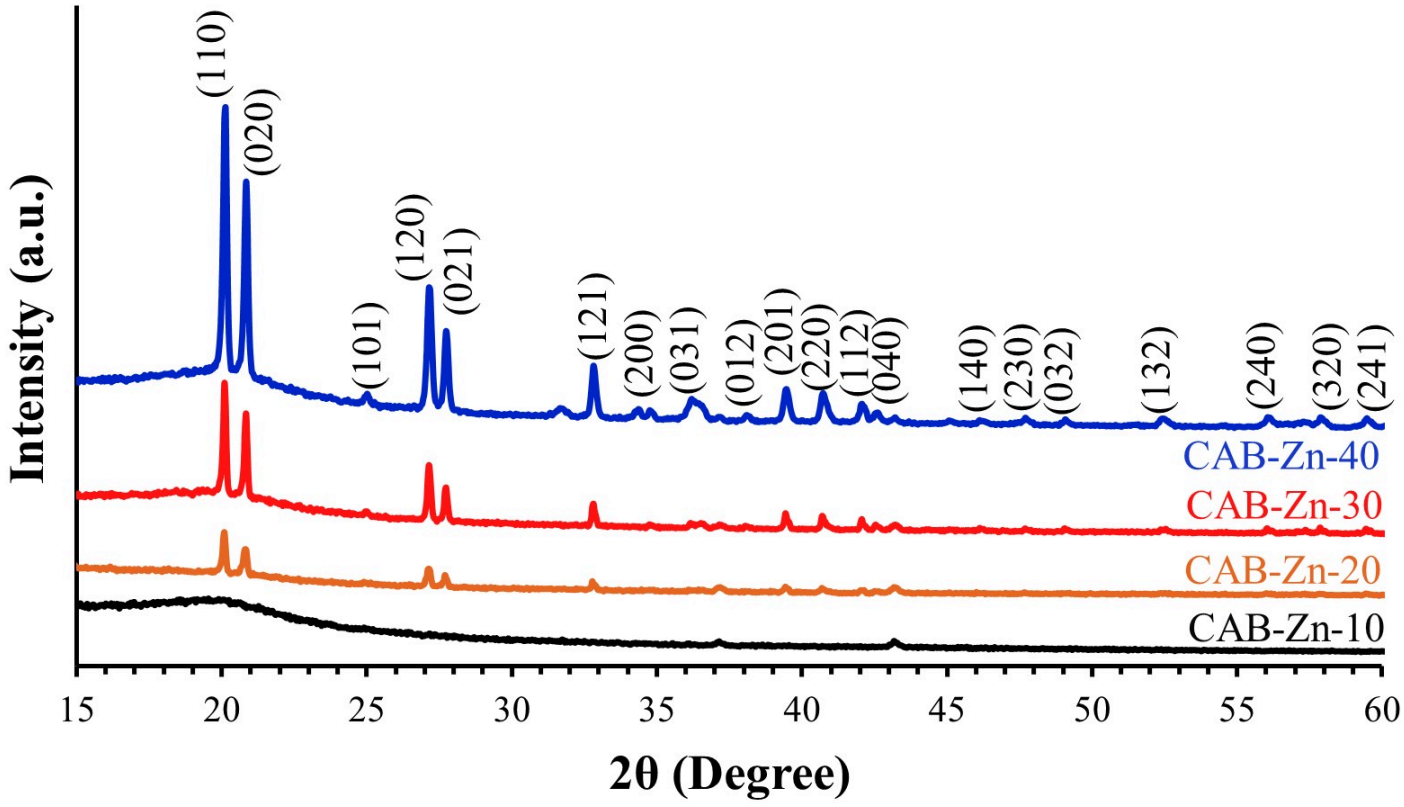

Figure 1

XRD patterns of CAB microcapsules coated with increasing concentrations of $Zn(OH)_2$. Changes in diffraction features with increasing $Zn(OH)_2$ content indicate the presence of zinc-containing phases and alterations in structural organization within the microcapsule system.

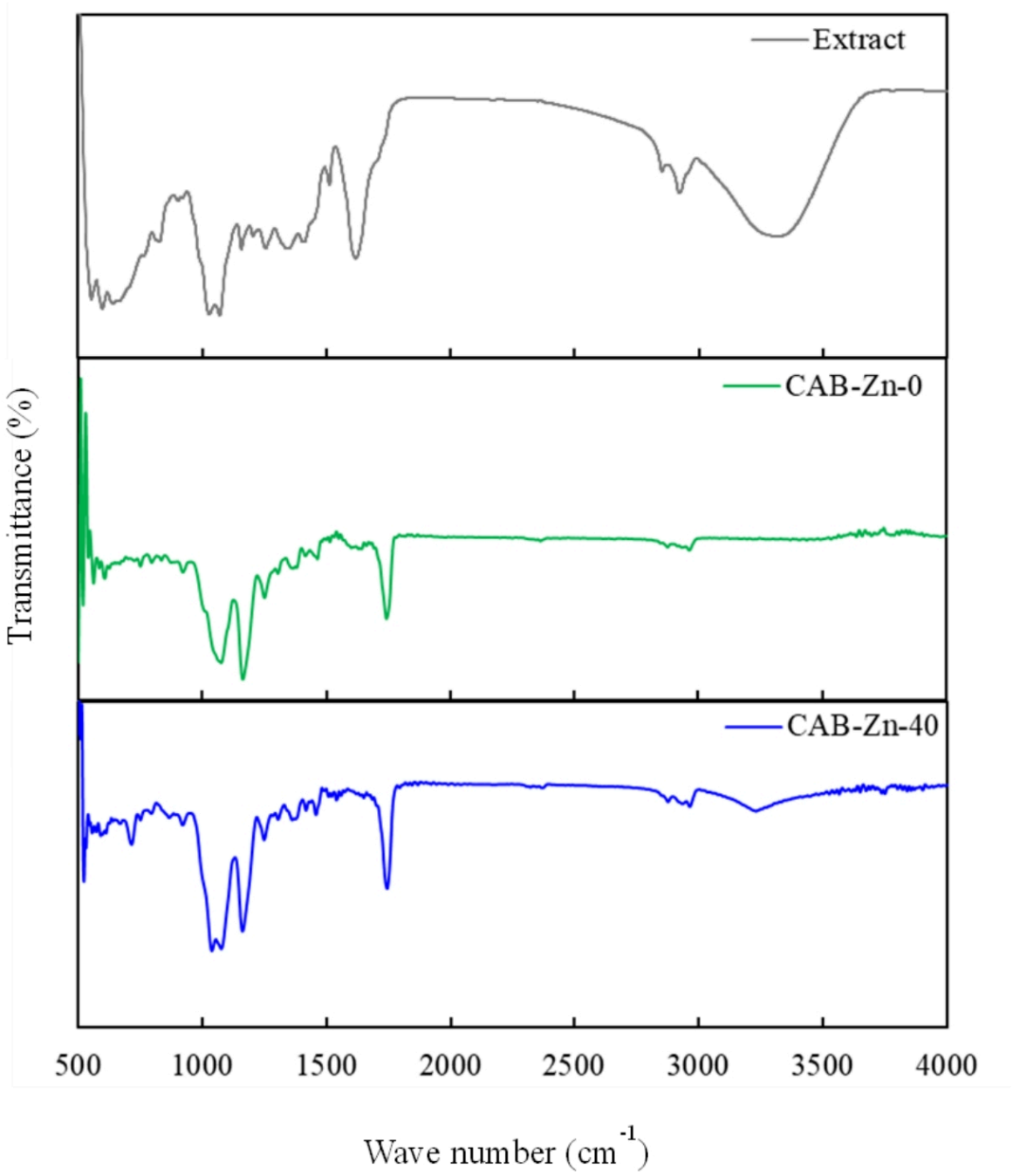

Figure 2

FTIR spectra of (a) crude *C. odorata* extract, (b) unmodified microcapsules (CAB–Zn–0), and (c) $Zn(OH)_2$-functionalized microcapsules (CAB–Zn–40). Variations in absorption bands indicate changes in the chemical environment of functional groups following $Zn(OH)_2$ incorporation and support the formation of an inorganic–organic hybrid microcapsule system.

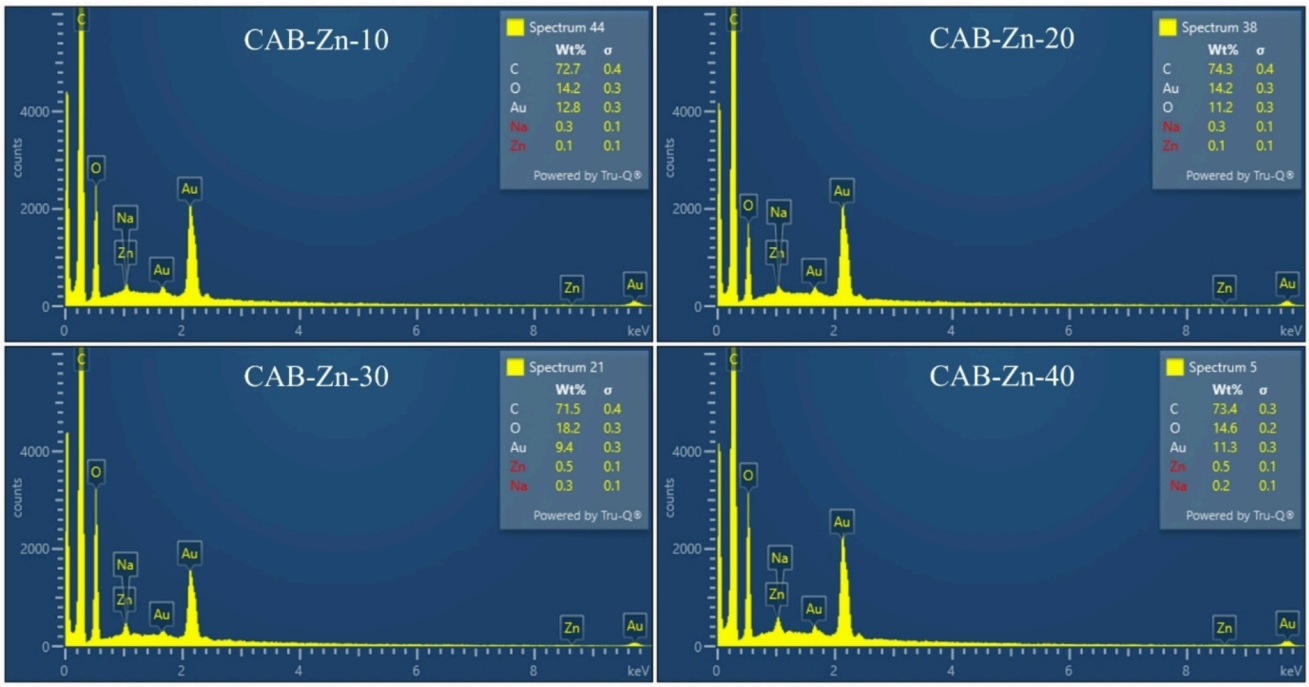

Figure 3

EDS spectra of $Zn(OH)_2$-coated *C. odorata*microcapsules. Detected elements include carbon (C), oxygen (O), and zinc (Zn), while gold (Au) originates from sputter coating. The presence of Zn signals indicates incorporation of zinc-containing components into the microcapsule system.

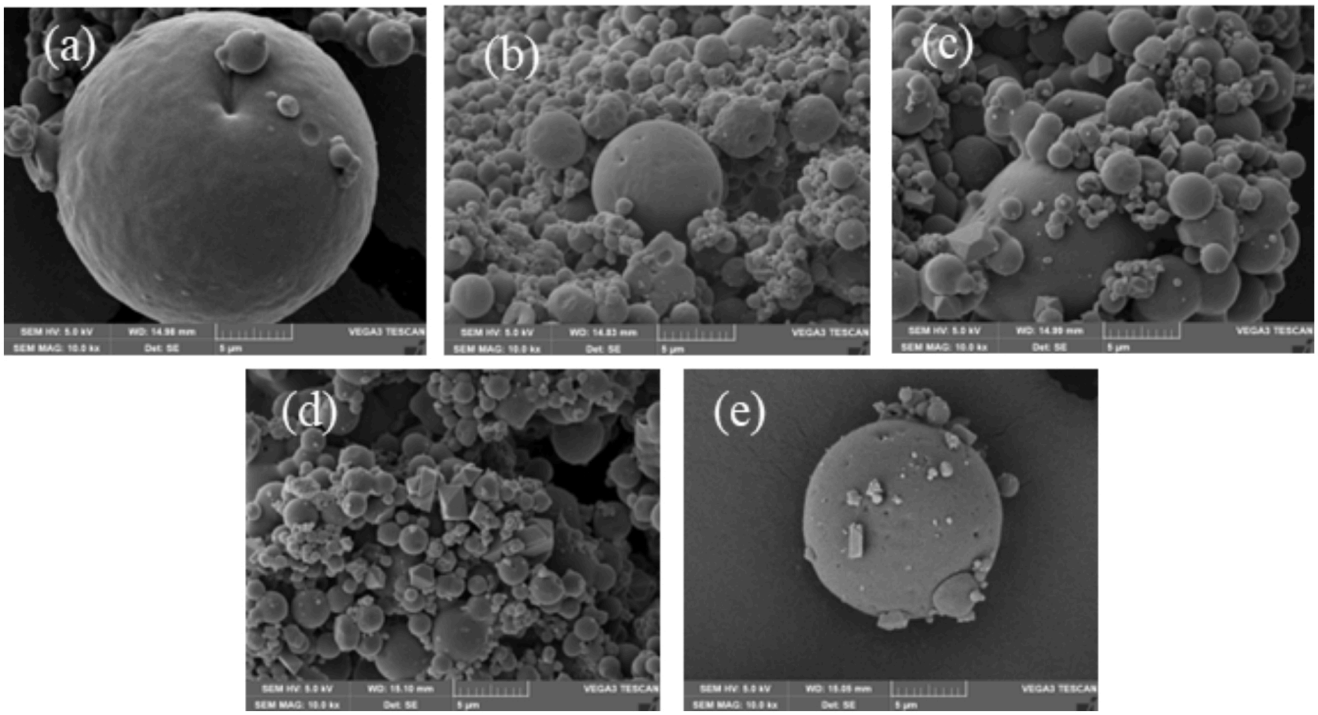

Figure 4

SEM micrographs showing the surface morphology of CAB microcapsules coated with increasing $Zn(OH)_2$ concentrations: (a) CAB–Zn–0 (uncoated), (b) CAB–Zn–10, (c) CAB–Zn–20, (d) CAB–Zn–30, and (e) CAB–Zn–40. Changes in surface morphology and particle coverage with increasing $Zn(OH)_2$ concentration suggest modification of microstructural characteristics.

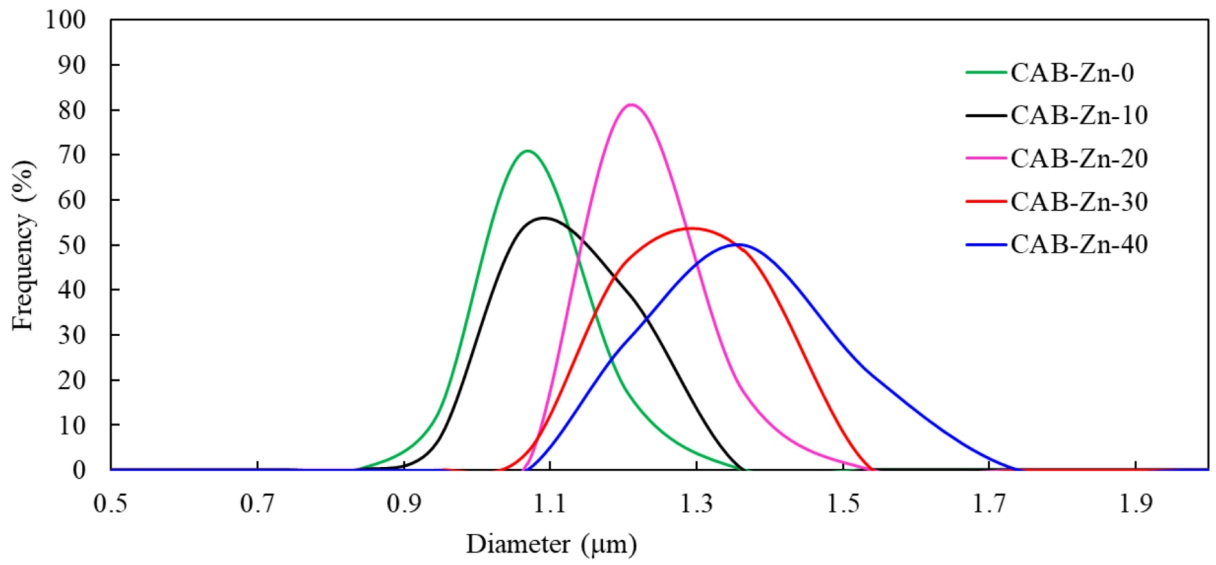

Figure 5

Particle size distribution profiles of CAB microcapsules coated with increasing $Zn(OH)_2$ concentrations. Variations in particle size distribution indicate that $Zn(OH)_2$ incorporation influenced microcapsule dimensions and dispersion characteristics.

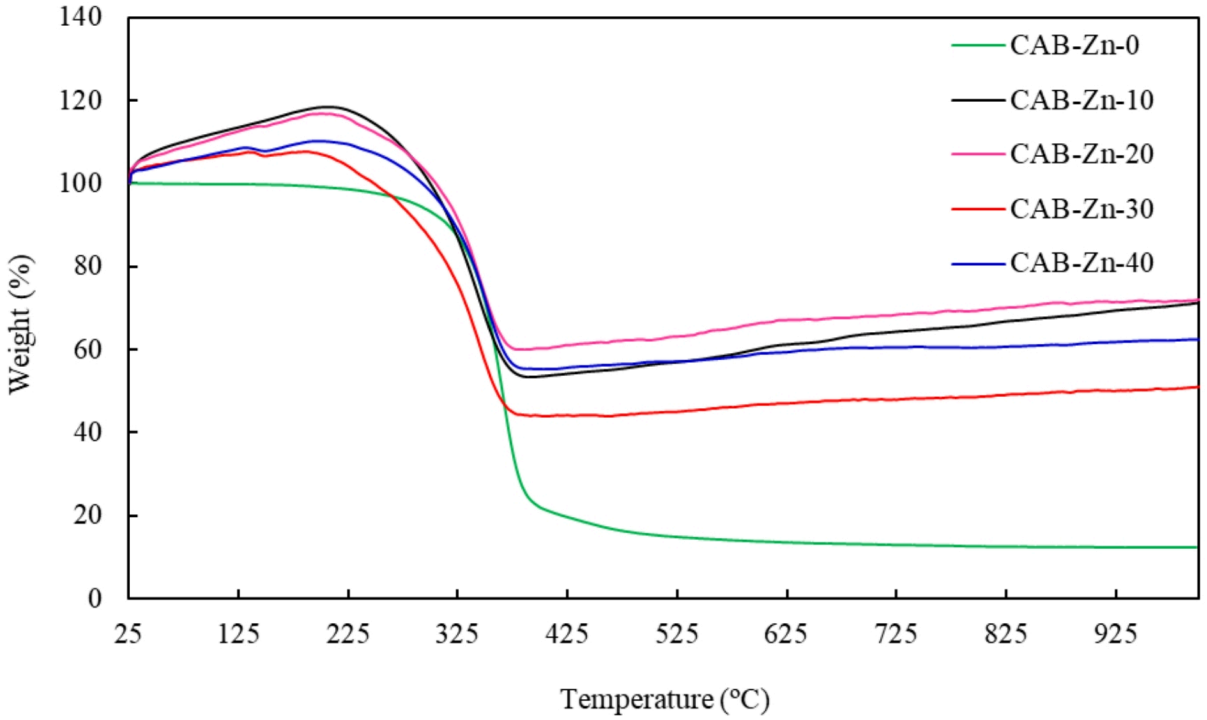

Figure 6

TGA thermograms of CAB microcapsules with and without $Zn(OH)_2$ coatings. Differences in thermal degradation behavior among formulations suggest that $Zn(OH)_2$ incorporation influenced thermal stability and decomposition characteristics.

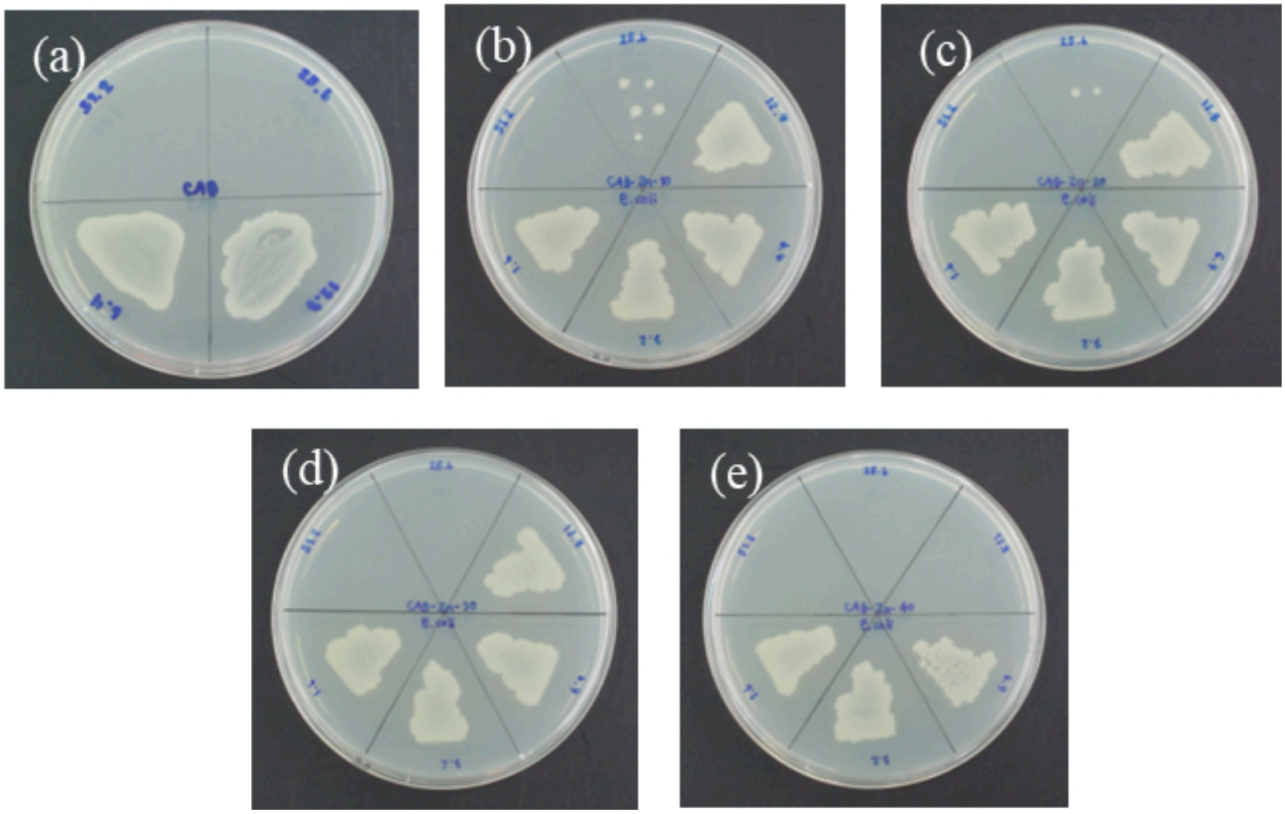

Figure 7

Minimum inhibitory concentration (MIC) values for CAB microcapsules with varying $Zn(OH)_2$ concentrations against *E. coli*and *S. aureus*. Differences in MIC values indicate that antibacterial activity varied with microcapsule composition and $Zn(OH)_2$ content.

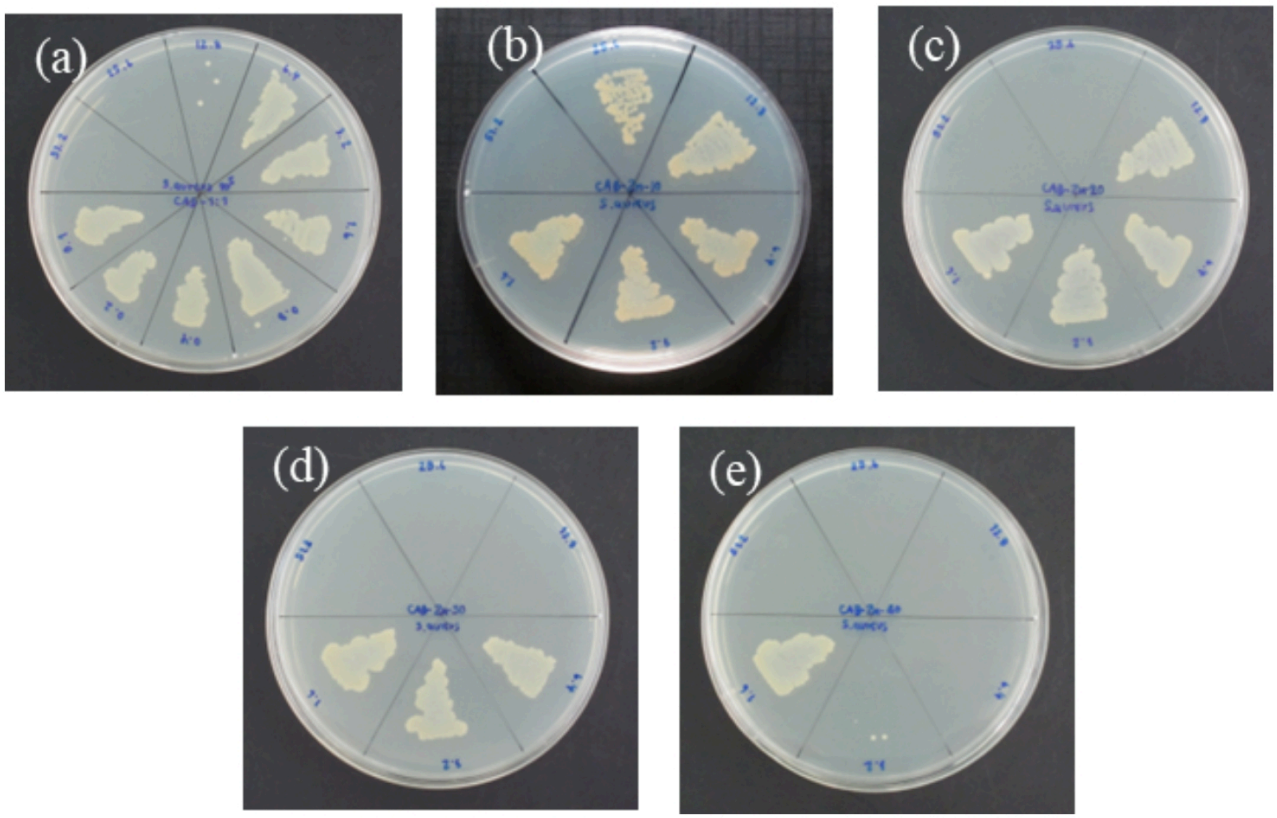

Figure 8

Representative spread plate images showing the antibacterial response of $Zn(OH)_2$-coated microcapsules against *S. aureus*. Reduced colony formation at selected concentrations is consistent with antibacterial activity observed in MIC and MBC measurements.

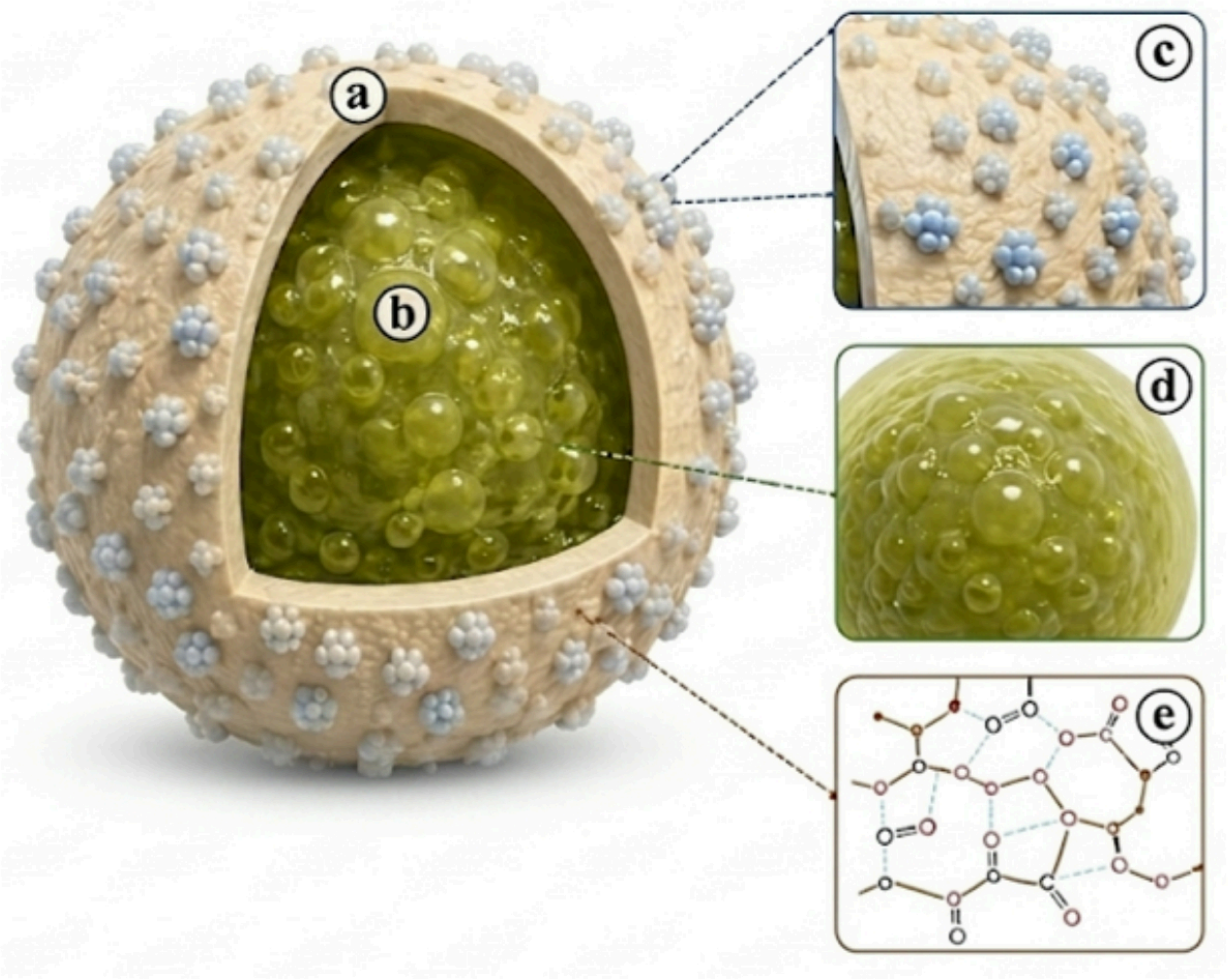

Figure 9

Proposed structural model of $Zn(OH)_2$-functionalized CAB hybrid microcapsules: (a) overall core–shell architecture of the hybrid microcapsule; (b) cross-sectional view showing the encapsulated *Chromolaena odorata* extract within the CAB matrix; (c) enlarged view of surface-associated $Zn(OH)_2$ domains; (d) schematic representation of the bioactive extract entrapped in the microcapsule interior; and (e) representative CAB structure illustrating possible physicochemical interactions within the hybrid system.